

# The Transient Evolution of Flow Due to the Excitation Pulse in Oscillating Drop Experiments in Microgravity Electromagnetic Levitation



GWENDOLYN P. BRACKER  and ROBERT W. HYERS

In oscillating drop experiments, surface oscillations in a molten sample are captured and analyzed to determine the surface tension and viscosity of a melt without the need to contact the liquid sample. In electromagnetic levitation, surface oscillations are initiated using an excitation pulse in the electromagnetic field. The variation in the electromagnetic force field drives rapid acceleration in the melt while also changing the flow pattern. During the quasi-static flow conditions prior to the excitation pulse, the flow displays a “positioner-dominated” flow pattern with 4 recirculation loops in the sample hemisphere. However, the accelerating flow of the excitation pulse transitions into a “heater-dominated flow” pattern in which there are only 2 recirculation loops in the sample hemisphere. Following the excitation pulse, the flow rapidly slows and quickly returns to the conditions present before the excitation pulse. For many combinations of parameters, the transition in the flow pattern results in a very complicated variation in velocity with time; that variation is the topic of this paper.

<https://doi.org/10.1007/s11661-023-07080-2>  
© The Author(s) 2023

## I. INTRODUCTION

**DURING** casting and additive manufacturing, it is essential that the fundamental properties of a melt are understood. In the case of casting capillaries, the melt must have a sufficiently low viscosity and surface tension to enter and flow into the capillaries. Other applications require information on the density and thermal expansion of the melt to efficiently process material. However, the high temperatures and high reactivity of many metallic melts present unique challenges to measuring such properties. Contactless processing is a set of techniques in which a metallic sample is isolated from the environment allowing such fundamental property measurements to be taken.

Samples are processed using contactless processing techniques such as electromagnetic levitation (EML) or electrostatic levitation (ESL). The metallic samples are

then melted using either a laser, as is often the case in ESL, or by applying the EML force field to the sample to induce Joule heating. One such facility, the International Space Station Electromagnetic Levitator (ISS-EML) described in Reference 1, further isolates the sample by processing in reduced gravity and significantly reducing the buoyancy forces acting on the melt.

Various experiments in EML require an understanding of the internal flow effects during measurements,<sup>[2,3]</sup> however, in the vast majority of EML experiments, it is not possible to directly measure the fluid flow in a sample. Sensors that require contact with the melt would be required to be chemically inert to the highly reactive melt while also withstanding the high temperatures necessary for metallic melts to be sustained in the liquid state. Further the surface of the metallic melts are opaque and featureless preventing particle-image-velocimetry. Therefore, magnetohydrodynamic modeling is the only technique that reliability provides insight into the flow within the melt. Insight into the internal flow of the drop requires magnetohydrodynamic models to link the experimental conditions with the thermophysical properties of the melt to calculate the forced flow within the drop. The results presented here use such magnetohydrodynamic models to evaluate the transient effects of excitation pulses, also commonly used during these experiments.

---

GWENDOLYN P. BRACKER is with the Institute for Materials Physics in Space, German Aerospace Center, 51147 Cologne, Germany and also with the Department of Mechanical Engineering, University of Massachusetts, Amherst, Amherst, MA 01002. Contact e-mail: [gwendolyn.bracker@dlr.de](mailto:gwendolyn.bracker@dlr.de) ROBERT W. HYERS is with the Department of Mechanical Engineering, University of Massachusetts, Amherst and also with the Department of Mechanical and Materials Engineering, Worcester Polytechnic Institute, Worcester, MA 01609.

Manuscript submitted January 13, 2023; accepted May 1, 2023.

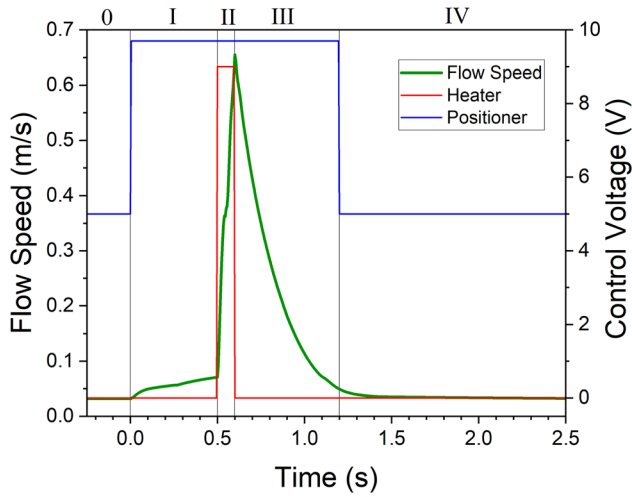


Fig. 1—In simple cases, like this modeled set of conditions, the flow smoothly accelerates and decelerates in response to the changes in the magnetic field. This case is calculated for a 9 V excitation pulse lasting 100 ms in an 8 mm sample with a viscosity of 10 mPa s and conductivity of  $5.4 \times 10^5$  S/m (Color figure online).

**Table I. Electrical Circuit Parameters for the ISS-EML Levitation Coils**

System Parameter	System Value
Heater Circuit Frequency ( $\omega_H$ )	$2\pi \times 372$ kHz
Positioner Circuit Frequency ( $\omega_{Pos}$ )	$2\pi \times 148$ kHz
Heater Circuit Capacitance ( $C_H$ )	$0.440 \times 10^{-6}$ F
Positioner Circuit Capacitance ( $C_H$ )	$2.50 \times 10^{-6}$ F

**Table II. Approximate Median Property Values for ISS-EML Experiments**

Property	Moderate Value
Sample Diameter	7.0 mm
Melt Conductivity	$2.77E+6$ S/m
Melt Density	$6900$ kg/m <sup>3</sup>
Melt Viscosity	10 mPa s
Pulse Height	6 V
Pulse Duration	0.2 s

### A. The Oscillating Drop Method

The oscillating drop method is an experimental technique for containerless processing in which the viscosity and surface tension of a melt are measured without contacting the molten material. Once the sample is melted at the desired temperature, the sample is excited to induce surface oscillations in the melt. The behavior of the surface oscillations is determined by the properties of the sample including the radius of the sample ( $R_0$ ), mass ( $m$ ), and melt density ( $\rho$ ). The surface tension, ( $\gamma$ ), determines the frequency, ( $f_1$ ) of the oscillations of mode (1) as described by Eq. [1].<sup>[3]</sup> Meanwhile, the melt viscosity, ( $\mu$ ) determines the damping coefficient for the oscillations ( $\tau_1$ ), given by Eq. [2].<sup>[4]</sup>

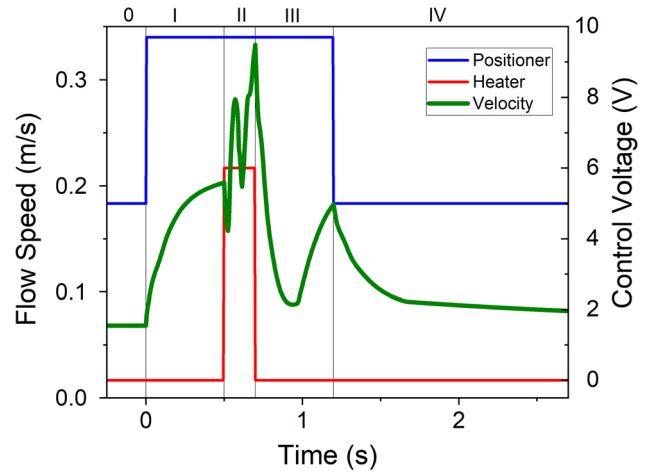


Fig. 2—In many cases, the flow response to the changing electromagnetic field is more complicated. While in stage I the flow is initially simple, during stage II the response is more complicated. The model plotted here has a melt viscosity of 10 mPa s and an electrical conductivity of  $2.77 \times 10^6$  S/m. The other parameters of this case are given in Table II (Color figure online).

$$f_1 = \left( \frac{l(l-1)(l+2)\gamma}{3\pi m} \right)^{1/2} \quad [1]$$

$$\tau_1 = \frac{\rho R_0^2}{(l-1)(2l+1)\mu} \quad [2]$$

The relationships derived by Rayleigh<sup>[3]</sup> and Lamb<sup>[4]</sup> assume that the melt is a force-free inviscid liquid, that the surface oscillations are very small compared to the radius of the sample, and that fluid flow within the drop is driven by the surface oscillations alone.

The model relating the oscillation behavior to the viscosity and surface tension has been expanded to encompass conditions like those in ESL and EML experiments. Lamb's work<sup>[4]</sup> provides for liquids with small viscosity values, while Reid and Suryanarayana in Reference 5 and 6 provide for melts with larger viscosities. Additionally, the assumption of infinitesimal oscillations has been shown to be satisfied when the amplitudes of the oscillations are less than 1 pct of the polar radius of the sample, while larger amplitude oscillations can still be used by applying empirical corrections.<sup>[7]</sup> Finally, flow within the drop is superimposed over any flow driven by the perturbations of the surface oscillations.

In the case of laminar flow, the flow does not seem to cause the momentum of the surface oscillations to be redistributed enough to affect the measurement. However, when turbulence is present in the flow, the turbulent viscosity redistributes the momentum the flow through turbulent eddies. By redistributing the momentum of the flow, the turbulent eddies effectively provide additional damping to the surface oscillations. As a result, the observed damping coefficient from Eq. [2] is the sum of damping provided by both the turbulent viscosity, a property of the flow, and the dynamic viscosity, a

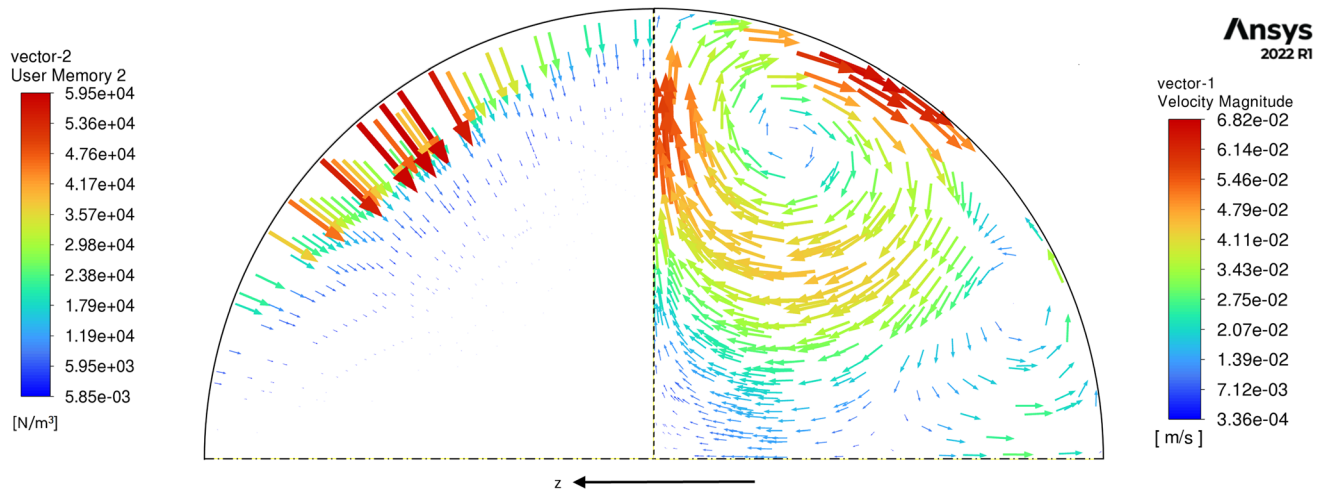


Fig. 3—Steady state: the EML force field (left) used during stable flight of the sample is 5 V positioner and 0 V heater. The resulting steady-state flow pattern (right) is positioner-dominated.

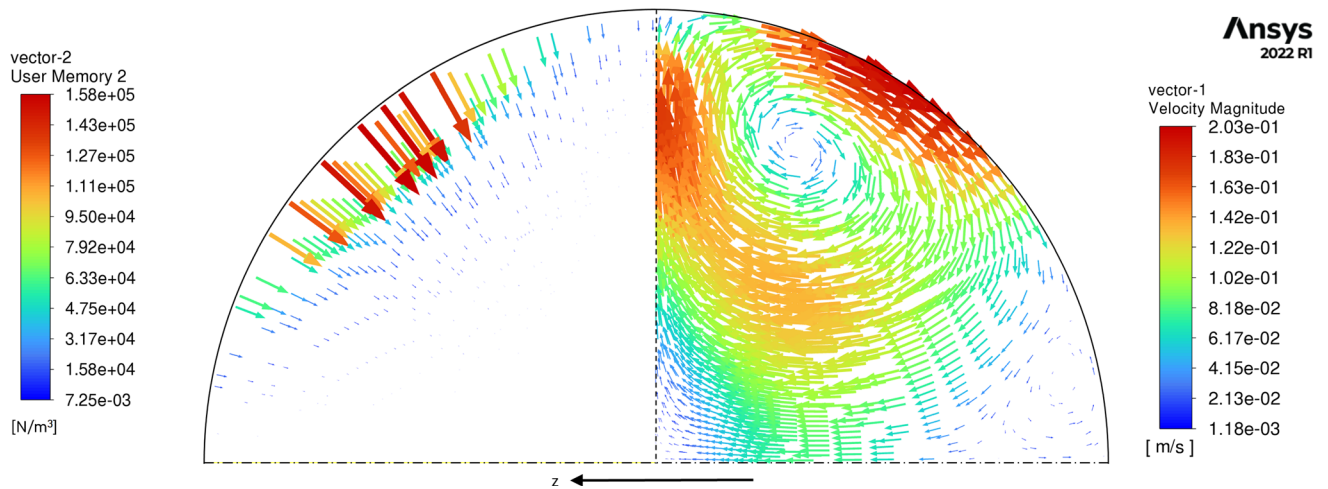


Fig. 4—Stage I: increased force field stiffness: a larger positioner field (left) is applied to stabilize the sample during the excitation pulse. It is generated by applying 9.7 V positioner and 0V heater. The positioner-dominated flow (right) is accelerated by the stronger EML field. The polar loop grows while the equatorial loop shrinks.

property of the melt. From this, it is recommended that the flow be calculated and characterized for the experimental conditions of any given study.<sup>[8]</sup>

### B. Flow During Driven by Excitations

During EML experiments, the surface oscillations are initialized by a brief spike in the force field which squeezes the sample around its equator. While the flow conditions during quasi-steady EML conditions have been studied at length,<sup>[2,8–13]</sup> the flow response to changing EML force fields has only recently been analyzed<sup>[14,15]</sup> for high viscosity and low conductivity melts such as  $Zr_{64}Ni_{36}$ , which has viscosity of 42 m Pa s and a conductivity of  $7.27 \times 10^5$  S/m.

Figure 1 demonstrates the simple transient flow response pattern of a hypothetical sample with a viscosity of 10 mPa s and conductivity of  $5.4 \times 10^5$  S/m. The simple flow response in the case here is similar to the prior published results and

provides the basis for discussion of the various stages of changes to the flow surrounding the excitation pulse. As in the other simple flow cases, the flow velocity (plotted in green) increases in response to a brief increase in the EML field which is controlled by the voltages applied to the levitation coils (plotted in red for the heater circuit and blue for the positioner circuit) in a sample.

Prior to the application of the excitation pulse, shown as stage I in Figure 1, the positioner field (which is proportional to the applied positioner voltage, given in blue) is increased to increase the stiffness of the magnetic field and control the movement of the sample. The flow responds to this change with a small increase in the velocity. The excitation pulse is applied (which is proportional to the applied heater voltage, given in red) and shown as stage II in Figure 1 and the flow rapidly accelerates during this period. Following the excitation pulse, the flow rapidly decelerates in stage III. Finally, the positioner field is reduced and the flow returns to the quasi-steady conditions prior to the excitation pulse during stage IV.

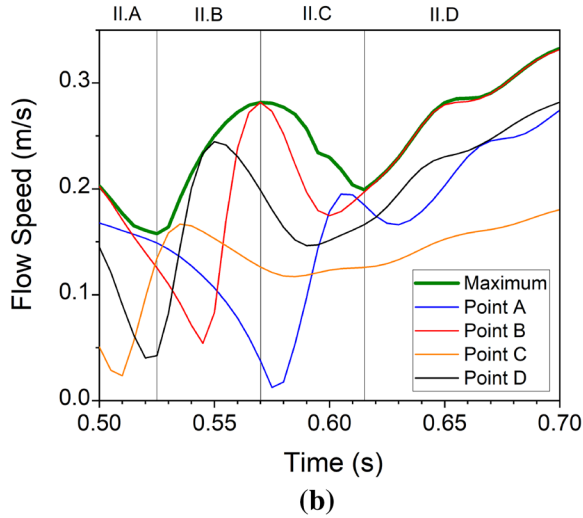
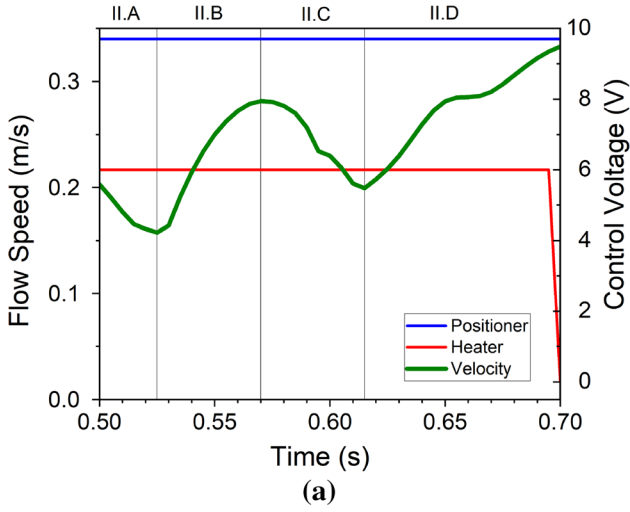


Fig. 5—In this model, the excitation pulse begins at elapsed time 0.50 s and last from 0.2 s to end at elapsed time 0.70 s. During the excitation pulse, the maximum velocity changes in a complicated manner due to the change in flow pattern from heater-dominated to positioner-dominated flow. (a) A more focused view of the maximum velocity during stage II shows the maximum velocity varies during the excitation pulse in a complicated way. (b) By tracking the velocity at different locations within the drop, the origin of the complicated shape of the maximum velocity is revealed. During the acceleration due to the excitation pulse, the location of the maximum velocity changes, suggesting that the flow pattern also changes.

While the flow's response to the changing velocity in Figure 1 is uncomplicated, other combinations of sample properties and excitation pulse parameters can result in much more complicated flow behavior during both acceleration and deceleration. Those more complicated behaviors are the subject of the present work.

## II. MODEL DETAILS

During electromagnetic processing, alternating current from a high frequency power supply flows through a coil system to produce a magnetic field. The magnetic

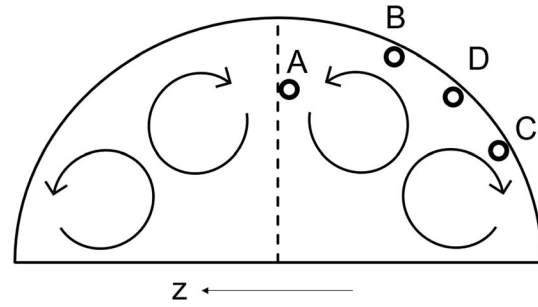


Fig. 6—Several points have been selected to investigate flow at these locations during the changes in flow patterns. Here, the points at which the instantaneous velocity is plotted in Figs. 5(b) and 9.

field, in turn, induces current within the sample and it is through this current that the sample is heated, by Joule heating, and supported, by Lorenz forces. Using the method of mutual inductions described in Reference 16, the applied forces and power are calculated as a functions of the coil geometry, applied currents, sample geometry, and sample properties.

The models here are calculating conditions present in ISS-EML experiments; thusly, the SUPOS coil geometry<sup>[1]</sup> is used in these calculations. This facility utilizes two superposed frequencies on the heater circuit and positioner circuit allowing the electromagnetic fields to be independently determined based on the control voltage applied to the high frequency power supply. The oscillating current traveling through the coils is calculated for each of the circuits according to Eqs. [3] and [4] at the given control voltage (CV) for the system parameters. The parameters for the ISS-EML are given in Table I. It is these currents that are the closest physical parameter to the strengths of the magnetic fields and induced currents. The magnetic model is used to calculate the applied forces and power to each discretized cell in conjunction with the surrounding cells from both magnetic fields. As a result, the distribution of the power and forces applied to the sample are known.

$$I_{H, Osc} = \omega_H C_H (17.95 x CV_H + 18.04(V)) \quad [3]$$

$$I_{Pos, Osc} = \omega_{Pos} C_{Pos} (17.95 x CV_{Pos} + 18.04(V)) \quad [4]$$

The forces from the above magnetic model are then coupled with a computational fluid dynamics solver to evaluate the flow driven by the said forces. In the computational fluid dynamics solver, the Navier–Stokes equations are evaluated to calculate the flow resulting from the sample geometry, melt properties, and forces applied to the system. In the models presented here, axial symmetry is used to reduce the computational intensity of the models. Additionally, in microgravity conditions, the molten sample is mirror-symmetric about the equator so the computations can be further reduced by cutting the axial hemisphere in half to give a quarter drop. These reductions of the computation

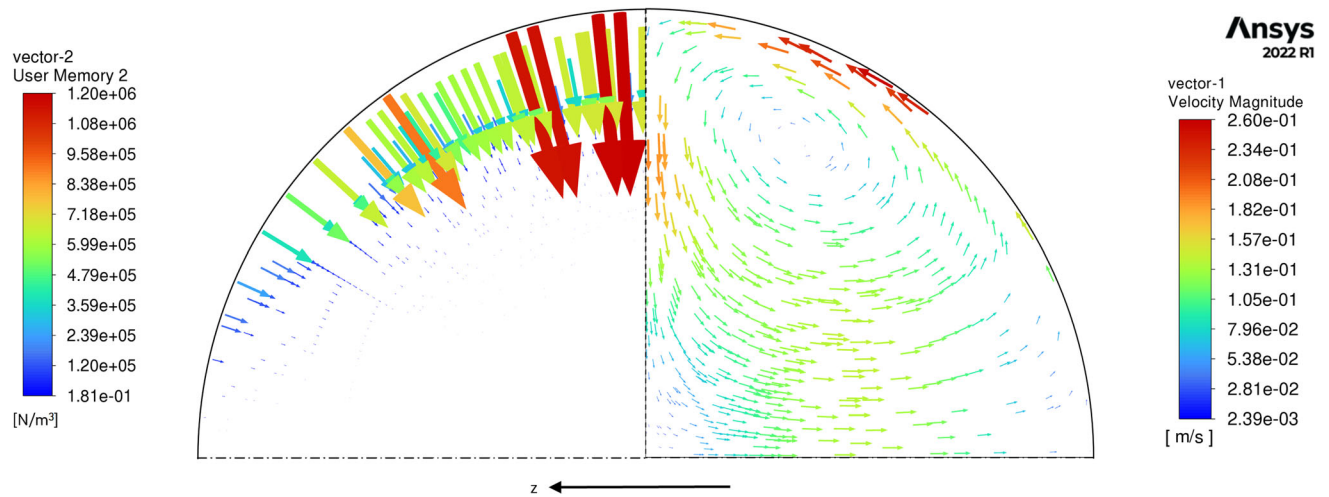


Fig. 7—Stage II: the excitation pulse: the surface oscillations are excited by the brief application of a large dipole field generated by the heater circuit (left). This field is generated using 9.7 V positioner and 6 V heater. During the pulse of the heater field, the flow is accelerated into a heater-driven flow pattern (right). This flow is taken at an elapsed time of 0.64 s near the end of the excitation pulse.

domain require symmetry boundaries at which the derivatives must be zero. Further, the surface of the molten sample must be free of traction and impermeable to the fluid.

During laminar flow, the Navier–Stokes equations are solved directly; however, when the flow is above the laminar–turbulent transition, the RNG  $k$ - $\epsilon$  model amends the Navier–Stokes equations by using the turbulent kinetic energy and turbulent rate of dissipation to estimate a local turbulent-eddy viscosity.

Further details on the magnetohydrodynamic models are discussed at length in Reference 14.

The model presented here evaluates the fluid flow during a median excitation pulse on a sample with median property values for those processed in the ISS-EML facility. These values are given in Table II. The model presented here evaluates the internal flow during a 6 V excitation pulse that is sustained for 200 ms. The oscillations in this sample would be expected to last for about 1.69 seconds according to 2 by Lamb. The expected time scale for viscous dissipation in this sample would be expected to be about 690ms, so about 41 pct of the oscillations that may be affected by the accelerated flow effects.

Flow is initiated in the model using the steady-state conditions prior to the excitation pulse. The excitation pulse is preceded and followed by an increase in the supporting positioner field. Following the pulse and the reduction of the stabilizing positioner field, the transient flow model computes that an additional 1.5 seconds is required for the flow to approach the new steady state.

### III. MODEL RESULTS AND DISCUSSION

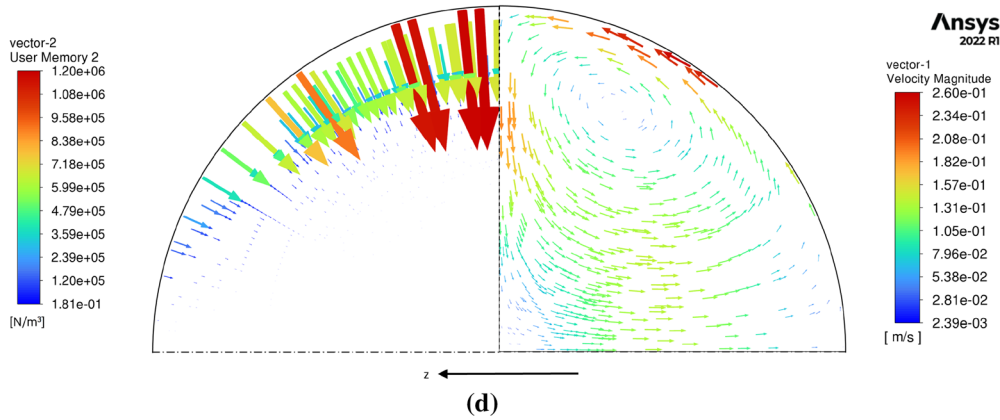
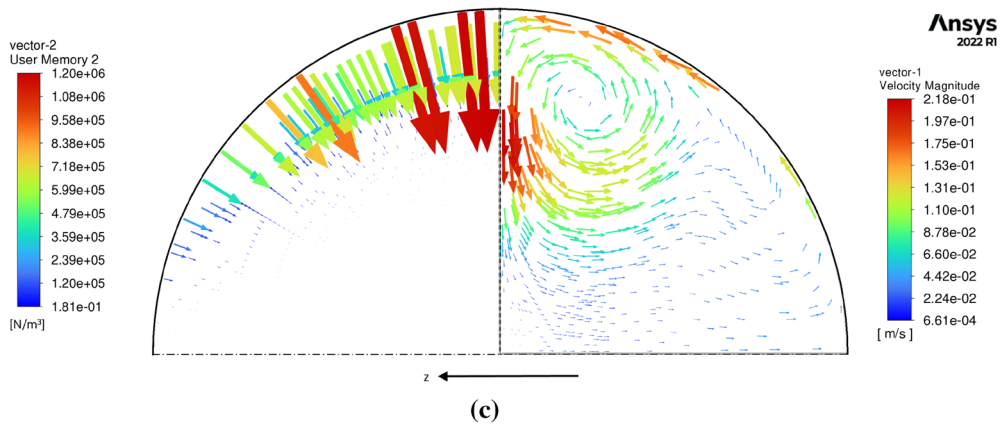
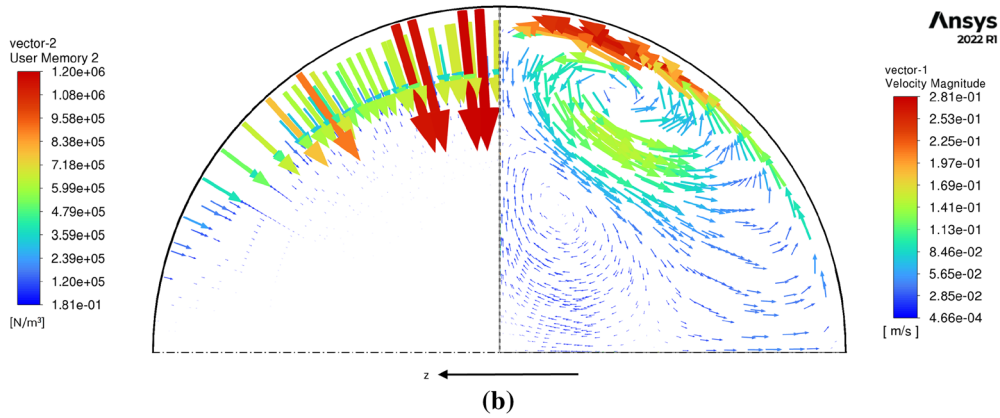
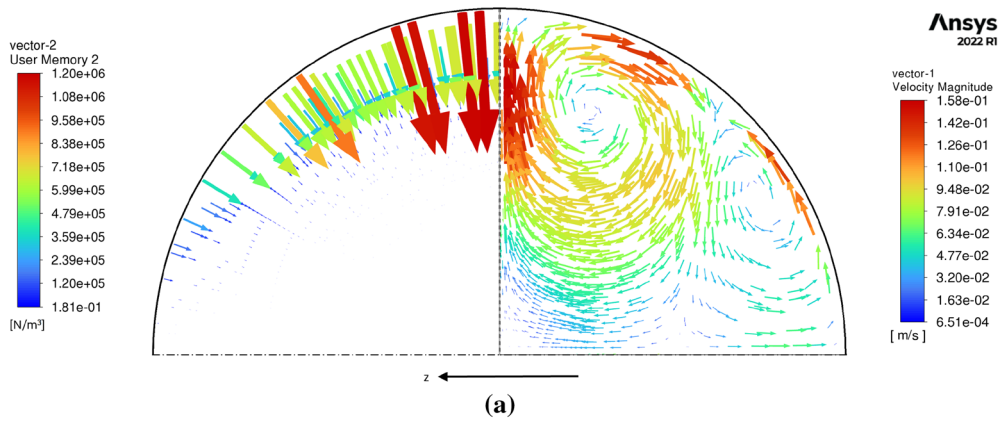
The results of the model are plotted Figure 2 in which the maximum velocity of the flow (green) is plotted over the duration of the excitation pulse which is given in red for the heater circuit and blue for the positioner circuit. The results have been divided into 4 stages for

discussion which are also given in Figure 2. The model is initiated with steady-state conditions prior to the excitation pulse. An increased positioner field in stages I–III increases the stiffness of the levitation field and stabilizes the sample. The excitation pulse itself occurs in stage II. The residual effects of the elevated positioner field and excitation pulse are observed in stage IV while the sample approaches the new steady-state conditions.

The model is initiated using the steady-state conditions plotted in Figure 2. The initial electromagnetic field is generated by applying 5 V to the positioner circuit and 0 V to the heater circuit. The forces applied to the molten sample are plotted in Figure 3 which shows a positioner-dominated electromagnetic force field with the largest forces applied along the surface of the sample at about  $\pm 45$  deg from the equator of the sample. The corresponding flow pattern is given in Figure 3 which features 2 recirculating loops in which melt is driven into the sample near  $\pm 45$  deg from the equator and returns to the surface along the equator and poles of the sample.

#### A. Stage I: Increased Force Field Stiffness

In this stage, the positioning field is increased prior to the excitation pulse. The stronger positioning field, shown as stage I in Figure 2, further stabilizes the sample prior to the excitation pulse. The case presented here uses 9.7 V in the positioner field and 0 V in the heater field to generate the forces plotted in Figure 4. The positioner-dominated force field applies the largest forces along the surface of the sample at about  $\pm 45$  deg from the equator of the sample. The EML force field generates a positioner-dominated flow pattern given in Figure 4 in which flow is driven to the interior of the sample near  $\pm 45$  deg from the equator and returns to the surface along the equator and poles of the sample. During this stage, the flow pattern remains positioner-driven but is accelerated from 6.8 to 20.3 cm/s by the larger EML force field. The Reynolds number



◀ Fig. 8—Stage II: The excitation pulse rapidly accelerates the flow and drives a pattern change. The flow pattern transitions from positioner-dominated flow to heater-dominated. (a) through (d) show samples of the flow evolution. (a) Stage II Part A: the polar recirculation loops increase in size and accelerate while the equatorial loops reduce in size and velocity. This image is taken at  $t = 0.525$  s, at the end of Stage II Part A. (b) Stage II Part B: The growing polar recirculation loop encounters the equatorial loop. The flow velocity traveling along the surface of the sample toward the equator increases. This snapshot is taken at  $t = 0.570$  s, at the end of Stage II Part B. (c) Stage II Part C: The equatorial recirculation loop is fully overtaken and the flow at the equator reverses direction. This image is taken at  $t = 0.605$  s, near the end of Stage II Part C. (d) Stage II Part D: The heater-dominated flow pattern has been fully established and flow accelerates within the flow pattern. This image is taken at  $t = 0.640$  s, in the middle of Stage II Part D.

analysis of the flow is discussed in Section III-E. During this acceleration, the flow exceeds the laminar-turbulent transition at Reynolds number 600 and likely becomes turbulent.

### B. Stage II: The Excitation Pulse

In this stage, the heating field is applied at a high level for a short period of time. The brief application of the heating field at a high level is referred to as the excitation pulse. This excitation pulse provides a large magnetic field around the equator of the sample to squeeze the sample and induce surface oscillations. Within the molten sample, the heater-dominated magnetic field drives rapidly accelerating flow while also forcing the flow to adopt a heater-dominated flow pattern.

The excitation pulse presented here uses features 6 V in the heater circuit sustained 0.2 second. In the heater-dominated EML force field, the forces are largest near the equator and along the surface of the sample. This larger EML force field drives rapid acceleration of flow within the sample, however, the fluid accelerates in a complex manner. Figure 5 shows an enlarged view of the maximum velocity in the drop during the excitation pulse.

In these investigations, the flow was evaluated at several locations in the sample to better understand the observed variations in the flow. The points used for this are given in Figure 6. Point A is located on the equatorial axis of symmetry around 2/3 the radius of the sample toward the surface. Points B and C are near the surface of the sample where the positioner-dominated recirculation loops travel parallel to the surface of the drop. Points B and C are 30 and 60 deg below the equator of the sample. Point D is placed along the surface of the sample at 45 deg below the equator. During positioner-dominated flow, point D is where the forces drive flow into the sample; however, in positioner-dominated flow the recirculation loop flows parallel to the surface of the sample at point D.

By observing the flow during the excitation pulse at multiple locations, (the locations are mapped to the drop in Figure 6) as is plotted for stage II in Figure 5(b), one can see that the location of the maximum velocity within the sample is moving. Additionally, the previously rapid flow in several regions of the sample slows

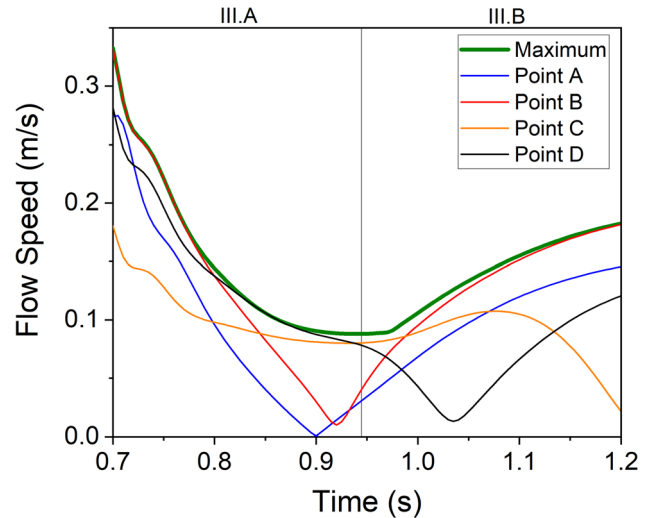


Fig. 9—In stage III, the pulse is over and the flow decelerates. The flow pattern changes toward the fast, positioner-dominated flow that is the equilibrium for the settings in staged I and IV. Here, the overall maximum velocity is plotted in green with the velocity in different parts of the sample (Color figure online).

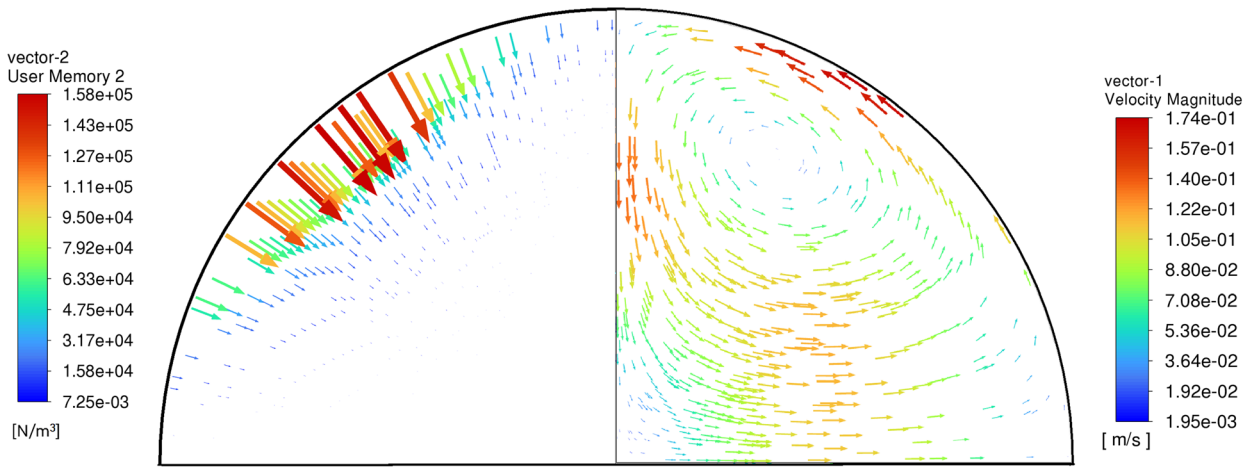
down, with some even changing direction. Such changes indicate that not only is the elevated magnetic field accelerating the fluid but is also inducing a change in the flow pattern from positioner-dominated flow to heater-dominated flow.

The large heater-dominated electromagnetic field is plotted with the heater-dominated flow pattern in Figure 7. During heater-dominated flow, flow is driven into the sample along the equator and returns to the surface near the poles of the sample. Unlike positioner-dominated flow, there are only 2 recirculation loops present in the sample hemisphere.

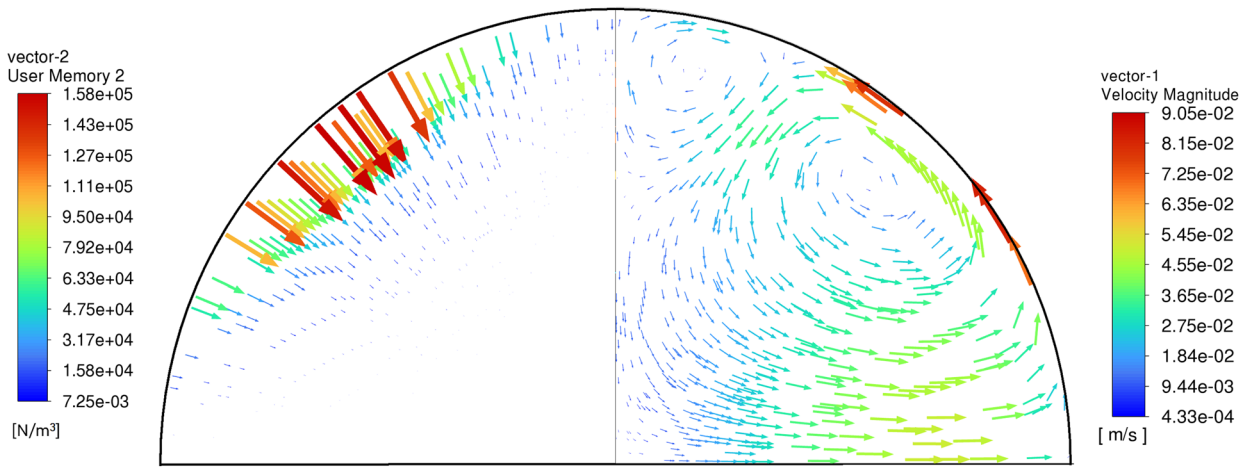
To better understand the development of the heater-dominated flow patterns, stage II is divided into four parts for discussion. Samples of the flow evolution in Figure 8 show the flow patterns at intermediate times in stage II. During stage II-A, the maximum velocity decreases while the circulation loops near the poles of the sample accelerate and increase in diameter at the expense of the equatorial loops.

Stage II-B, Figure 8(b), begins as the growing polar recirculation loops collide with those near the equator of the sample. During stage II-B, the maximum velocity occurs near the surface of the sample, moving from point C to D to B due to the increased momentum of the growing polar recirculation loop. In stage II-C, Figure 8(c), the polar recirculation loops finish overtaking the smaller loops near the equator of the sample. As this overtaking is completed, the former equatorial loop disappears. The flow is now inward at the equator, replacing the outward flow from the positioner-dominated condition. Meanwhile, the flow at the equator of the sample changes directions to flow toward the interior of the sample and away from the large forces applied by the EML force field.

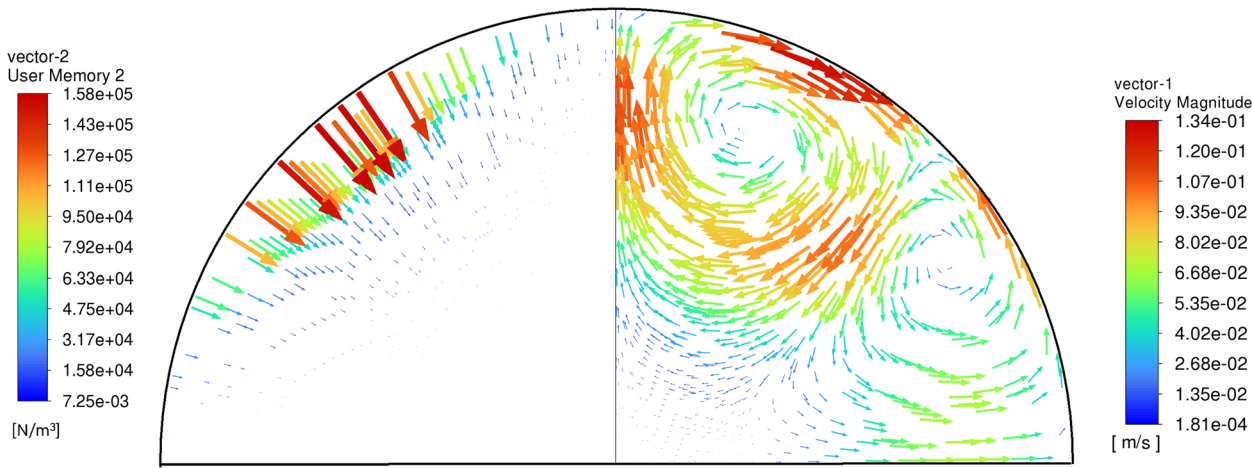
Stage II-D, Figure 8(d) is composed of the acceleration of the flow in a stable heater-dominated flow



z ← (a)



z ← (b)



z ← (c)



◀Fig. 10—The flow pattern changes during stage III as the flow decelerates after the excitation pulse. The new pattern is positioner-dominated flow. (a) Stage III Part A: The flow decelerates in response to the changing electromagnetic force field. This image is taken at  $t = 0.775$  s toward the end of Stage III Part A. (b) At the interface between Stage III Part A and Part B, the flow reverses direction at the equator and an equatorial recirculation loop forms. This image is taken at  $t = 0.900$  s near the end of Stage III Part A. (c) Stage III Part B: The flow stabilizes in a positioner-dominated flow pattern and accelerates. This image is taken at  $t = 1.050$  s during the end of Stage III Part B.

pattern. The heater-dominated flow pattern continues to accelerate through the remainder of the excitation pulse and the momentum of the flow continues into the beginning of stage III.

### C. Stage III: Deceleration under High Positioning Forces

In this stage, the excitation pulse is completed; however, the positioning force remains elevated to maintain control of the sample. As in stage I, the electromagnetic force field is generated by applying 9.7 V to positioner circuit and 0 V to the heater circuit. The generated forces on the sample are plotted in Figure 4.

During this time, the flow rapidly decelerates and transitions back to positioner-dominated flow. As in the transition to heater-dominated flow, the maximum velocity does not smoothly decelerate but again evolves in a more complex manner reflecting the changing flow directions and locations of maximum velocity. The maximum velocity is plotted with the flow velocities at various locations in the drop in Figure 9, where the velocities at the various locations show the flow accelerating and decelerating in varying locations.

During stage III part A, the flow slows in response to the reduced force fields, Figure 10(a). In Figure 9, the flow velocity at all plotted locations rapidly decreases. The magnitude of the velocity approaches 0 m/s at point A and near point B, which is consistent with the directional change required to change from heater-dominated to positioner-dominated flow. As the flow slows, flow begins to be driven into the sample around  $\pm 45$  deg from the equator of the sample and additional recirculation loops form along the equator of the sample. The formation of these loops is shown in Figure 10(b). In stage III part B, the positioner-dominated flow pattern stabilizes. Once the new flow pattern has stabilized, the flow accelerates in a positioner-dominated flow pattern like that shown in Figure 10(c).

### D. Stage IV: Return to Steady-State Flow Conditions

In this final stage, the positioner current is reduced to allow the positioner field to return to the same level as before the pulse, 5 V. However, the flow retains momentum that is still to be dissipated in stage IV of Figure 2. The forces applied to the sample are consistent with those present during the steady-state conditions, given in Figure 3. During stage IV, the velocity vectors

are initially larger as the flow decelerates; however, the flow returns to the steady-state conditions, which are given in Figure 3.

### E. Flow Analysis

In this base case, the peak flow velocity was 33.3 cm/s, which gives a Reynolds number of 1607, which is well above 600, the laminar-turbulent transition for microgravity EML samples.<sup>[10]</sup> The flow, in this case, accelerates above the laminar-turbulent transition during stage I with the elevation of the positioner field after only 75 ms. The flow remains clearly above the laminar-turbulent transition through stage II of the excitation pulse into stage III. During heater-dominated flow, the flow pattern has 2 recirculation loops in a given hemisphere of the sample with flow being driven toward the interior of the sample at the equator. The diameter of these recirculation loops is approximately the same as the radius of the sample. In this 750 ms period, particles at the peak flow speed have the opportunity to travel around the recirculation loop more than 22 times, providing ample opportunities for instabilities in the flow to develop and propagate. During stage III, the flow slows below the laminar-turbulent transition for 210 ms during the transition from heater-dominated to positioner-dominated flow. However, the flow subsequently does briefly accelerate in stage III B to be above the laminar-to-turbulent transition for an additional 150 ms before slowing below a Reynolds number of 600 to stay. During this brief period of acceleration, the peak flow velocity is 18.3 cm/s. The flow pattern during this period is positioner-dominated in which the diameter of the recirculation loops can be approximated to be  $2/3$  the radius of the sample. From this the flow may travel around the recirculation loops about 12 times. In stage IV, the flow rapidly slows. Only 300 ms after the removal of the elevated positioner field, the acceleration of the flow is approaching steady state under the new condition.

## IV. CONCLUSIONS

In some cases like those discussed in Reference 14, the excitation pulse does not drive sufficient acceleration in the flow to induce turbulence. The model presented here illustrates that in other conditions within the range common to ISS-EML experiments, the excitation pulse drives flow that not only accelerates above the laminar-turbulent transition but also causes a complex change in the flow pattern. While the maximum velocity in the sample shows several minima and maxima, these are artifacts of the pattern change in which the location of greatest flow velocity changes location to accommodate new flow directions and magnitudes. In experiments with different conditions, such as the intensity and duration of the excitation pulse, viscosity of the melt, electrical conductivity, and even sample size may respond differently to the excitation pulse and other changes to the levitation field.

## ACKNOWLEDGMENTS

The authors acknowledge collaborate support by team members from the Microgravity User Support Center (MUSC) through access to the ISS-EML facility which is a joint undertaking of the European Space Agency (ESA) and the German Aerospace Administration (DLR). Support for this project was provided to the USTIP project through NASA Grants NNX16AB40G and 80NSSC21K0103.

## CONFLICT OF INTEREST

On behalf of the authors, the corresponding author states that there are no conflicts of interest.

## FUNDING

Open Access funding enabled and organized by Projekt DEAL.

## OPEN ACCESS

This article is licensed under a Creative Commons Attribution 4.0 International License, which permits use, sharing, adaptation, distribution and reproduction in any medium or format, as long as you give appropriate credit to the original author(s) and the source, provide a link to the Creative Commons licence, and indicate if changes were made. The images or other third party material in this article are included in the article's Creative Commons licence, unless indicated otherwise in a credit line to the material. If material is not included in the article's Creative Commons licence

and your intended use is not permitted by statutory regulation or exceeds the permitted use, you will need to obtain permission directly from the copyright holder. To view a copy of this licence, visit <http://creativecommons.org/licenses/by/4.0/>.

## REFERENCES

1. G. Lohöfer and J. Piller: in *Proceedings 40th AIAA Aerospace Sciences Meeting and Exhibit*, 2002.
2. A.K. Gangopadhyay, M.E. Sellers, G.P. Bracker, D. Holland-Moritz, D.C. Van Hoesen, S. Koch, P.K. Galenko, A.K. Pauls, R.W. Hyers, and K.F. Kelton: [arXiv:2103.16439](https://arxiv.org/abs/2103.16439) [cond-mat], 2012.
3. L. Rayleigh: *Proc. R. Soc. Lond.*, 1879, vol. 29, pp. 71–97.
4. H. Lamb: *Proc. Lond. Math. Soc.*, 1881, vol. s1-13(1), pp. 51–70.
5. W.H. Reid: *Proc. Lond. Math. Soc.*, 1960, vol. 18(1), pp. 86–89.
6. P.V.R. Suryanarayana and Y. Bayazitoglu: *Int. J. Thermophys.*, 1991, vol. 12(1), pp. 137–51.
7. X. Xiao, R.W. Hyers, R.K. Wunderlich, H.-J. Fecht, and D.M. Matson: *Appl. Phys. Lett.*, 2018, vol. 113(1), p. 011903.
8. G. Bracker, E. Baker, J. Nower, M. Sellers, A. Gangopadhyay, K. Kelton, X. Xiao, J. Lee, M. Reinartz, S. Burggraf, D. Herlach, M. Rettenmayr, D. Matson, and R. Hyers: *High Temp. High Press.*, 2019, vol. 49(1), pp. 49–60.
9. R.W. Hyers, D.M. Matson, K.F. Kelton, and J.R. Rogers: *Ann. N. Y. Acad. Sci.*, 2004, vol. 1027(1), pp. 474–94.
10. R.W. Hyers, G. Trapaga, and B. Abedian: *Metall. Mater. Trans. B*, 2003, vol. 34B, pp. 29–36.
11. J. Lee, D.M. Matson, S. Binder, M. Kolbe, D. Herlach, and R.W. Hyers: *Metall. Mater. Trans. B*, 2014, vol. 45B, pp. 1018–23.
12. R. W. Hyers: *Meas. Sci. Technol.*, 2005, vol. 16(2), pp. 394–401.
13. X. Xiao, R.W. Hyers, and D.M. Matson: *Int. J. Heat Mass Transf.*, 2019, vol. 136, pp. 531–42.
14. G. Bracker and R. Hyers: *High Temp. High Press.*, 2023, vol. 52(2), pp. 111–122.
15. G. Bracker, S. Schneider, D. Matson, and R. Hyers: *Materialia*, 2022, vol. 26, p. 101623.
16. J.-H. Zong, J. Szekely, and E. Schwart: *IEEE Trans. Magn.*, 1992, vol. 28(3), pp. 1833–42.

**Publisher's Note** Springer Nature remains neutral with regard to jurisdictional claims in published maps and institutional affiliations.